A Journal of the Gesellschaft Deutscher Chemiker

Angewandte International Edition GDCh Chemie

www.angewandte.org

Accepted Article

Title: Oriented Ultrathin π-complexation MOF Membrane for Ethylene/Ethane and Flue Gas Separations

Authors: Yanwei Sun, Shen Hu, Jiahui Yan, Taotao Ji, Liangliang Liu, Mingming Wu, Xinwen Guo, and Yi Liu

To be cited as: *Angew. Chem. Int. Ed.* **2023**, e202311336

Link to VoR: https://doi.org/10.1002/anie.202311336

WILEY VCH

RESEARCH ARTICLE

WILEY-VCH

Oriented Ultrathin π-complexation MOF Membrane for Ethylene/Ethane and Flue Gas Separations

Yanwei Sun,[a] Shen Hu,[a, b] Jiahui Yan,[a] Taotao Ji,[a] Liangliang Liu,[a] Mingming Wu,[a] Xinwen Guo,[a] and Yi Liu*[a, c]

[a] Dr. Y. Sun, Dr. S. Hu, J. Yan, T. Ji, L. Liu, M. Wu, Prof. Dr. X.Guo, Prof. Dr. Y. Liu
State Key Laboratory of Fine Chemicals, Frontiers Science Center for Smart Materials, School of Chemical Engineering
Dalian University of Technology
Dalian, 116024, China
E-mail: diligenliu@dlut.edu.cn

[b] Dr. S. Hu
Sinopec Nanjing catalyst co., ltd
Nanjing, 210000, China

[c] Prof. Dr. Y. Liu
Dalian Key Laboratory of Membrane Materials and Membrane Processes
Dalian University of Technology
Dalian, 116024, China

Supporting information for this article is given via a link at the end of the document.

Abstract: Rational design and engineering of high-performance molecular sieve membranes towards C_2H_4/C_2H_6 and flue gas separations remain a grand challenge to date. In this study, through combining pore micro-environment engineering with meso-structure manipulation, highly *c*-oriented sub-100 nm-thick Cu@NH_2-MIL-125 membrane was successfully prepared. Coordinatively unsaturated Cu ions immobilized in the NH_2-MIL-125 framework enabled high-affinity π-complexation interactions with C_2H_4, resulting in an C_2H_4/C_2H_6 selectivity approaching 13.6, which was 9.4 times higher than that of pristine NH_2-MIL-125 membrane; moreover, benefiting from π-complexation interactions between CO_2 and Cu(I) sites, our membrane displayed superior CO_2/N_2 selectivity of 43.2 with CO_2 permeance of 696 GPU, which far surpassed the benchmark of other pure MOF membranes. The above multi-scale structure optimization strategy is anticipated to present opportunities for significantly enhancing the separation performance of diverse molecular sieve membranes.

Introduction

Membrane-based separation has shown obvious superiority in terms of carbon footprint, energy efficiency, and capital cost.[1] As a new type of ordered microporous material, metal-organic framework (MOF) holds great potential to provide high selectivity and permeability because of its tunable pore aperture for precise molecular sieving and rich functionality for preferential adsorption.[2] Nevertheless, MOF membranes still suffer from an upper bound limitation on their separation performance[3]. Manipulation of the pore microenvironment (e.g., pore size, adsorption properties, and defective sites) of MOF membranes at the sub-nanometer scale has been proven to exert a profound influence on their separation performance, relying on the mechanism of molecular sieving or preferential adsorption.[4] Regarding molecular sieving, the separation performance is mainly determined by pore size. Nevertheless, intrinsic flexibility of the MOF framework renders it difficult to predict molecular sieving capability, thus posing a grand challenge for accurate separation of gas mixtures with extremely close kinetic diameters. For instance, accurate C_2H_4/C_2H_6 separation, although being significant, remains quite challenging due to the subtle difference in their kinetic diameters (0.028 nm). As a result, the C_2H_4/C_2H_6 selectivity of state-of-the-art MOF membranes commonly falls below 10;[5] in addition, MOF membrane-based flue gas separation, which represents an import step towards CO_2 capture, rarely achieved a CO_2/N_2 selectivity higher than 40 to date, owing to their similar physicochemical properties.[6]

A potential solution to this challenge is to design selective recognition sites featuring electronic interactions with guest molecules. It has been reported that transition metal ions can form π-complexation interaction with the double bonds of gas molecules.[7] Therefore, immobilization of coordinatively unsaturated metal ions capable of selective π-complexation with π-electron-rich molecules such as C_2H_4 and CO_2 represents an effective strategy to improve their adsorption selectivity. For instance, Bloch et al. reported that Fe(II) open sites could interact with olefin molecules by donating π-bonded electrons from olefin molecules to Fe(II) open sites, resulting in high C_2H_4/C_2H_6 selectivity of Fe-MOF-74.[8] Later this strategy was extended to the incorporation of Ag(I) and Cu(I) over MIL-100 and MIL-101, respectively, giving rise to remarkable enhancement in adsorption affinity for C_2H_4, and therefore, improved C_2H_4/C_2H_6 selectivity.[9] In addition to MOF materials, Shang et al. further prepared Co^{2+} and Ni^{2+}-exchanged SSZ-13 for CO_2/N_2 separation, relying on d_π-d_π back donation from transition metal cations to CO_2.[10] Nonetheless, to the best of our knowledge, there have been no report on the fabrication of selective pure MOF membranes through π-complexation interaction.

In addition to pore microenvironment engineering, meso-structure control (e.g., grain boundary structure, crystallographic orientation, and thickness) represents another crucial factor for modulating MOF membrane separation performance.[11] Previous studies revealed that highly oriented ultrathin MOF membranes commonly exhibited superior separation performance due to concurrent minimization of non-selective grain boundary defects and diffusion path length.[12] In view of this, we envisioned a breakthrough in MOF membranes separation performance through multi-scale structure optimization (e.g., coupling π-complexation micro-environment with oriented ultrathin meso-structure).

MIL-125, which is representative of titanium-based MOF materials, consists of octahedra $Ti_8(\mu2\text{-}O)_8(\mu2\text{-}OH)_4$ nodes connected by terephthalate linkers.[13] NH_2-MIL-125 shares an identical topology with MIL-125. Owing to its appropriate pore size, strong affinity with CO_2, and excellent stability, NH_2-MIL-125 has been deemed as an ideal candidate for high-performance CO_2-permselective membranes.[14] Tremendous efforts have been devoted to manipulating the meso-structure of NH_2-MIL-125 membranes through coupling oriented seed layer deposition with in-plane epitaxial growth. Following this route, recently we prepared highly *c*-oriented 500 nm-thick NH_2-MIL-125 membrane.[15] Nonetheless, it remained impractical to further reduce its thickness to a sub-100 nm scale, owing to the difficulty in decreasing the thickness of the seed layer and preventing its excessive epitaxial growth. Simultaneously, we noticed that in the NH_2-MIL-125 framework, NH_2-BDC linkers were able to complex with transient metals[16], thus forming preferential binding sites capable of selectively discriminating C_2H_4 and CO_2 via reversible π-complexation interaction. Through combining with meso-structure manipulation, we anticipated that NH_2-MIL-125 membranes with superior C_2H_4/C_2H_6 and CO_2/N_2 separation performance could be achieved.

Motivated by the above concerns, in this study, we explored the preparation of highly *c*-oriented sub-100 nm-thick NH_2-MIL-125 membrane chelated with coordinatively unsaturated Cu ions (denoted as Cu@ORI-MIL-M), which was achieved through nanosheet (NS) seed preparation, oriented seed monolayer deposition, and coordination modulated epitaxial growth (Figure 1). On the microscopic scale, $-NH_2$ groups warranted single Cu ions to be anchored on the framework, facilitating the π-complexation interaction with C_2H_4 and CO_2, and therefore, higher C_2H_4/C_2H_6 and CO_2/N_2 selectivity; on the mesoscopic scale, employing copper acetylacetonate ($Cu(acac)_2$) as growth modulator was found crucial for the formation of ultrathin Cu@NH_2-MIL-125 NS seeds and membranes, leading to enhanced gas permeance. Owing to the multi-scale structure superiority, both C_2H_4/C_2H_6 and CO_2/N_2 separation performances of our membrane ranked the highest among pure MOF membranes.

Results and Discussion

The first step involved solvothermal synthesis of NH_2-MIL-125 seeds chelated with coordinatively unsaturated Cu ions (denoted as Cu@NH_2-MIL-125) via coordination-modulated reaction with $Cu(acac)_2$ as both growth modulator and copper source. As shown in Figure 2a, uniform square-shaped NSs with an average thickness of 70 nm and aspect ratio of 9.2 were formed under optimized solvothermal conditions. EDXS mapping demonstrated homogeneous distribution of Cu elements in Cu@NH_2-MIL-125 framework (Figure 2b), and no visible sign of Cu nanoparticles was observed in the TEM image, thus revealing a high dispersion of Cu species. The XRD pattern of Cu@NH_2-MIL-125 NSs was in good accordance with the simulated XRD, further confirming that prepared NSs were pure NH_2-MIL-125 phase (Figure 2c).[17] The peaks assignable to scissoring and rocking vibrations of $-NH_2$ were observed at 1686 and 1110 cm^{-1} (Figure 2d) in the FT-IR spectrum, while the peak shift confirmed the existence of strong interactions between Cu ions and dangling $-NH_2$ groups. In addition, no new peaks assignable to the vibration of Cu-O bonds in the spectrum could be discerned, implying that Cu ions were not incorporated in NH_2-MIL-125 framework.

Chemical states of both N and Cu elements in Cu@NH_2-MIL-125 framework was further characterized by XPS. As shown in Figure 2e, the binding energy of the N 1s photoelectrons of Cu@NH_2-MIL-125 NSs shifted towards a higher position (399.6 eV) compared with that of NH_2-MIL-125 (399.5 eV), demonstrating the formation of positively charged N species, which was consistent with FT-IR results. In addition, as shown in Figure 2f, characteristic signals derived from Cu(I) at binding energies of 940.9 and 933.2 eV, corresponding to Cu 2p 1/2 and 2p 3/2 bonds, were observed in the XPS spectrum of Cu@NH_2-MIL-125 NSs, confirming the successful introduction of Cu(I) sites, which was beneficial for reversible complexation and efficient recognition of C_2H_4 and CO_2; while the Cu 2p 3/2 peak

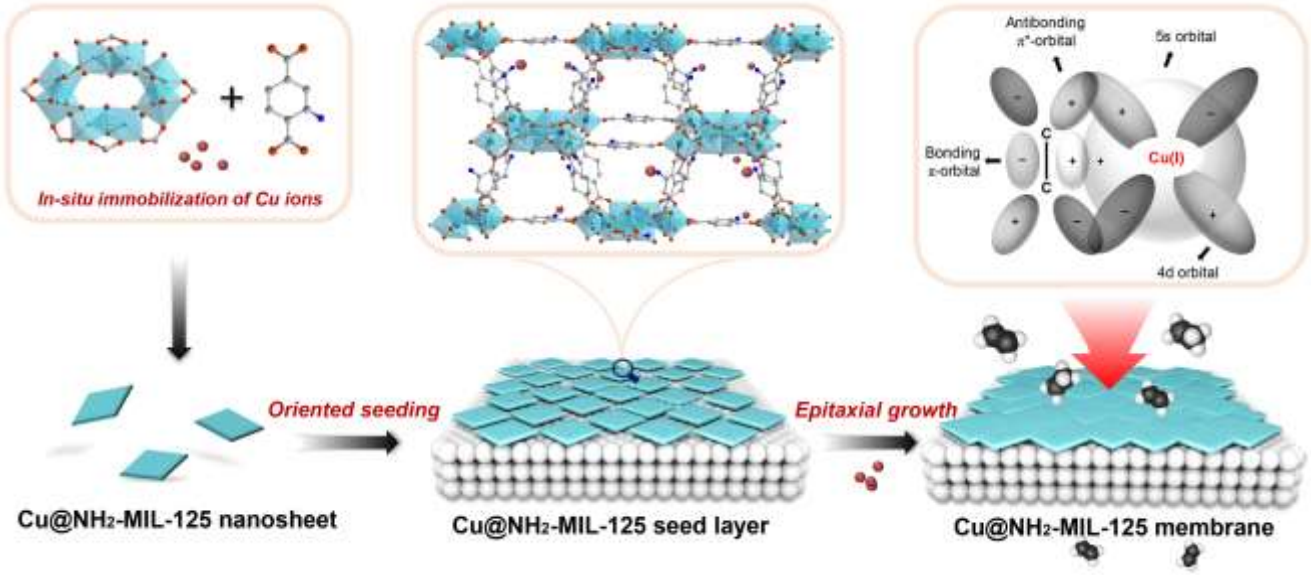

Figure 1. Scheme illustration of the preparation of highly *c*-oriented ultrathin π-complexation Cu@NH_2-MIL-125 membrane.

at 934.8 eV and 2p-to-3d shake-up line around 944.5 eV could be assigned to Cu(II) in Cu@NH_2-MIL-125 NSs. The above results convincingly demonstrated the presence of both Cu(I) and Cu(II). Further calculation by curve-fitting showed that Cu(I) accounted for ~43% of all Cu species in Cu@NH_2-MIL-125. We inferred that methanol may act as the reducing agent for in-situ reduction of Cu(II) to Cu(I) as convinced by previous studies. For instance, Sun et al. prepared zeolite Y chelated with Cu(I) sites by introducing methanol as the reducing agent to reduce Cu(II) to Cu(I).[18]

Our results indicated that $Cu(acac)_2$ may serve as modulator during NS formation. For comparison, we found that the thickness of NH_2-MIL-125 seeds significantly increased to 250 nm in the absence of $Cu(acac)_2$ while keeping all other synthetic conditions unchanged. The reduction in thickness could be ascribed to effective manipulation of growth rates in different lattice directions. Previous studies indicated that lowering precursor concentration enabled inhibition of the growth vertical to (001) plane in NH_2-MIL-125 framework.[19] In this study, since Cu^{2+} and Ti^{4+} were in competition in terms of coordination with NH_2-BDC ligands, the concentration of $Ti_8O_8(OH)_4(COO)_{12}(NH_2)_6$ secondary building units (Ti_8-oxo SBUs) was equivalently reduced through adding Cu^{2+} in the precursor solution, resulting in the formation of ultrathin NH_2-MIL-125 NSs.

We further studied the textural properties of Cu@NH_2-MIL-125 NSs. N_2 adsorption/desorption isotherms of Cu@NH_2-MIL-125 NSs revealed type I isotherm, indicating the presence of micropores (Figure 3a), while the BET surface area reached 1092 $m^2\ g^{-1}$, which was comparable with that of NH_2-MIL-125 powders prepared in the absence of $Cu(acac)_2$ modulator (1110 $m^2\ g^{-1}$). In contrast, after the introduction of Cu ions, both their micropore volume and pore size decreased from 0.50 $m^3\ g^{-1}$ and 5.8 Å to 0.45 $m^3\ g^{-1}$ and 5.6 Å, respectively, possibly owing to partial pore blockage by Cu species (Figure 3b).

To further quantify their affinity interactions with chelated Cu(I) sites, C_2H_4 and C_2H_6 adsorption isotherms of Cu@NH_2-MIL-125 NSs were measured. In the absence of Cu(I), adsorption capacities of C_2H_4 and C_2H_6 of NH_2-MIL-125 powders synthesized without addition of $Cu(acac)_2$ were similar (Figure 3c); in contrast, Cu@NH_2-MIL-125 NSs exhibited preferred C_2H_4 adsorption with an uptake capacity of 4.28 mmol g^{-1} at 298 K and 1.0 bar, resulting in significantly enhanced C_2H_4/C_2H_6 IAST selectivity from 1.1 to 4.6 (Figure 3d). Obviously, immobilizing Cu(I) sites in the framework was beneficial for enhancing C_2H_4/C_2H_6 separation performance of the membrane. To gain insight into the role of Cu ions in gas adsorption, molecular simulations were performed based on density functional theory (DFT) method.[20] Our studies revealed that both C_2H_4 and C_2H_6 were localized in a triangular pocket formed by three NH_2-BDC linkers, and more specifically, adjacent to Cu(I) sites. It was worth noting that the C-Cu distance between C_2H_4 and the framework (2.01 Å) was shorter than that for C_2H_6 (3.24 Å) (Figure 3e-f), resulting in a notable difference in the binding energy (-1.382 eV and -0.394 eV for C_2H_4 and C_2H_6, shown in Figure 3g), indicating that Cu(I) sites had a stronger affinity for C_2H_4 than C_2H_6. We also noticed that the binding energy between C_2H_4 and Cu@NH_2-MIL-125 was more negative than that for NH_2-MIL-125 (-0.041 eV), confirming that the creation of chelated Cu(I) sites effectively strengthened interactions between π-electron-rich molecules and the NH_2-MIL125

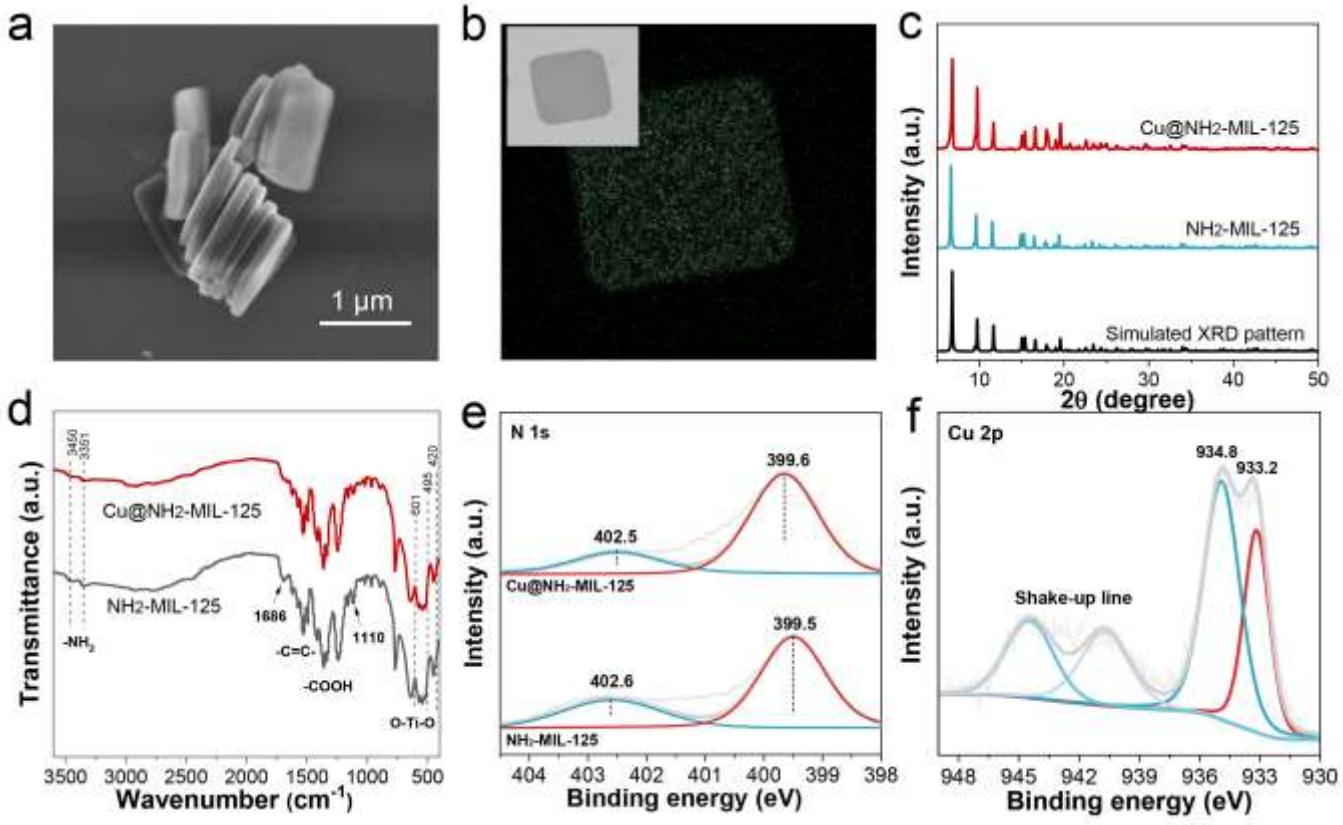

Figure 2. Characterization of Cu@NH_2-MIL-125 NSs. a) SEM image, b) TEM image and EDXS element mapping of Cu element in Cu@NH_2-MIL-125 NSs, c) XRD patterns and d) FT-IR spectra of Cu@NH_2-MIL-125 NSs and NH_2-MIL-125 crystals. XPS spectra of e) N1s and f) Cu 2p in Cu@NH_2-MIL-125 NSs.

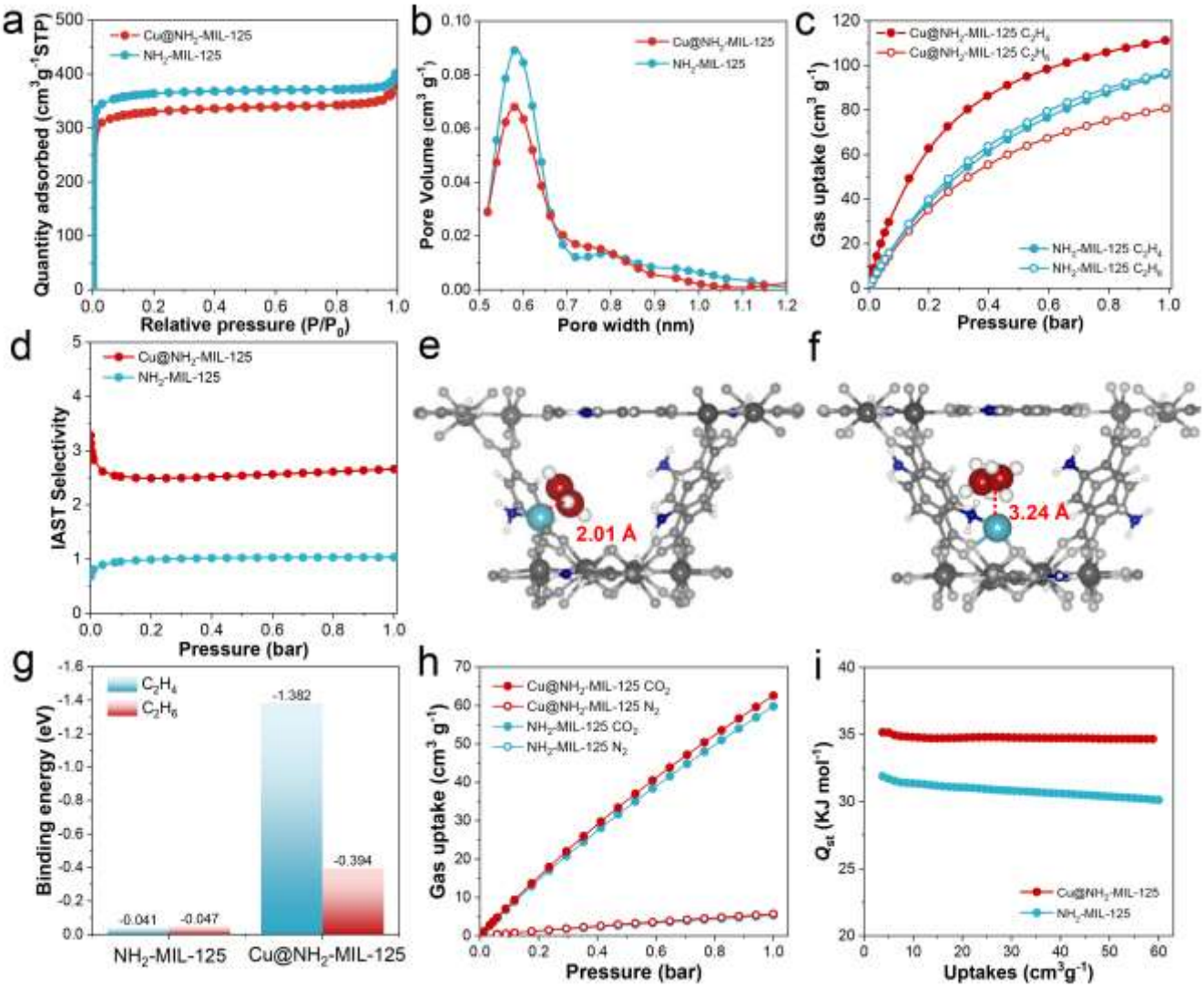

Figure 3. Textural properties of Cu@NH_2-MIL-125 NSs. a) N_2 sorption isotherms, b) pore size distributions, c) C_2H_4 and C_2H_6 adsorption isotherms (298 K), and d) C_2H_4/C_2H_6 IAST selectivity of Cu@NH_2-MIL-125 NSs and NH_2-MIL-125 crystals. Optimized binding sites of Cu@NH_2-MIL-125 with e) C_2H_4 and f) C_2H_6 molecules and g) calculated binding energy. h) CO_2 and N_2 adsorption isotherms (298 K) and i) isosteric adsorption heats of CO_2 on Cu@NH_2-MIL-125 NSs and NH_2-MIL-125 crystals as a function of uptake.

framework.

In terms of the affinity for CO_2, compared with NH_2-MIL-125, Cu@NH_2-MIL-125 exhibited a certain enhancement in CO_2 adsorption capacity, while the N_2 adsorption capacity remained largely unchanged (Figure 3h), implying preferential CO_2 adsorption of chelated Cu(I) sites. To evaluate the interaction strength between CO_2 and Cu@NH_2-MIL-125, the isosteric heat of adsorption (Q_{st}) was calculated using the Clausius-Clapeyron equation by fitting the CO_2 adsorption isotherms at 273 and 298 K. As expected, the Q_{st} value of CO_2 in Cu@NH_2-MIL-125 was much higher than that in NH_2-MIL-125 (Figure 3i, S1), confirming the affinity interplay between CO_2 and the framework was enhanced[21], which was beneficial for achieving higher CO_2/N_2 selectivity.

Subsequently, Cu@NH_2-MIL-125 NSs were deposited on porous α-Al_2O_3 substrate (Figure 4a) through the dynamic air-liquid-interface-assisted self-assembly method developed in our group. Relevant SEM image demonstrated the formation of uniform and closely packed Cu@NH_2-MIL-125 NS monolayer with a thickness of ~70 nm (Figure 4b, Figure S2). The dominance of preferred *c*-orientation was confirmed by the XRD pattern since only (002) and (004) diffraction peaks were present (Figure 4f).

The next step involves epitaxial growth of *c*-oriented seed layers. Being analogous to MOFs, in recent decades significant progress was made in the epitaxial growth strategy for the fabrication of oriented zeolite membranes. For instance, Tsapatsis et al. prepared ultrathin *b*-oriented MFI membranes by using gel-free method.[22] Nevertheless, the controllable epitaxial growth of oriented seed layer for the fabrication of ultrathin-oriented MOF membrane still remains quite limited**.** Herein, coordination-modulated epitaxial growth[23], referring to the addition of competitive coordinating modulators during the epitaxial growth, was performed under convective heating for sealing intergranular gaps in the seed layer. After epitaxial growth, a well-intergrown membrane with few twins could be obtained. As reported in our previous study, twin generation in *c*-oriented NH_2-MIL-125 film could be effectively suppressed by introducing competitive metal ion as coordination modulator. In

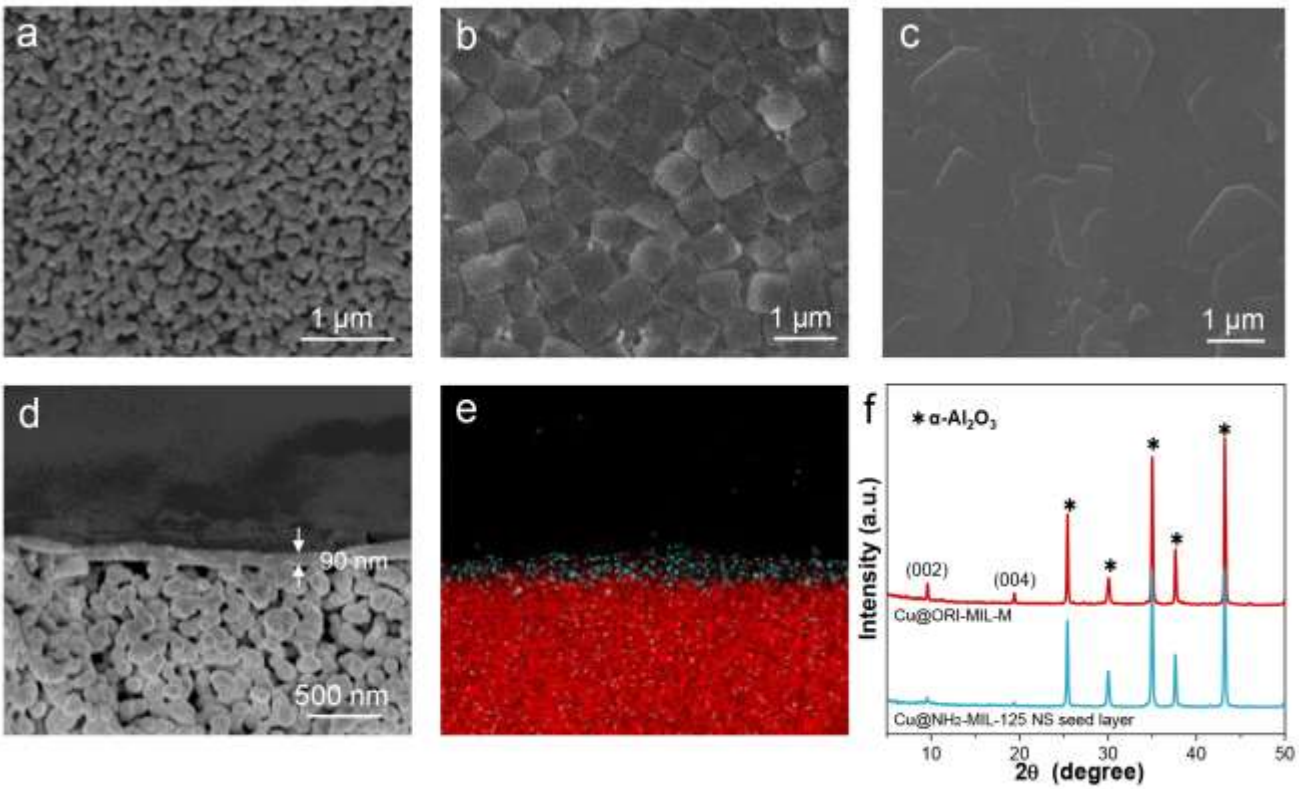

Figure 4. Characterization of Cu@NH_2-MIL-125 seed monolayer and membrane. SEM images of a) porous α-Al_2O_3 substrate and b) Cu@NH_2-MIL-125 NS seed layer on porous α-Al_2O_3 substrate. c) top and d) cross-sectional views of Cu@ORI-MIL-M prepared by modulated epitaxial growth under single-mode microwave heating. e) EDXS mapping of Cu (colour code: green) and Al (colour code: red) distributions at the cross-section of the prepared Cu@ORI-MIL-M. f) XRD patterns of Cu@NH_2-MIL-125 NS seed layer and Cu@ORI-MIL-M on porous α-Al_2O_3 substrate.

this study, the addition of an appropriate amount of Cu ions enabled the equilibrium concentration of Ti_8-oxo SBUs below the nucleation threshold, thus prohibiting homogenous nucleation in the bulk solution. Nevertheless, its thickness sharply increased to 250 nm (Figure S3), which could be attributed to excessive epitaxial growth in the vertical direction. Our previous study indicated that in comparison with conventional heating, employing single-mode microwave heating during MOF membrane growth enabled not only suppression of nucleation in the bulk solution but also promotion of growth rate in the lateral direction, resulting in the formation of ultrathin membrane without sacrificing continuity.[12c,14b] In this study, single-mode microwave-assisted coordination-modulated epitaxial growth was employed for the fabrication of Cu@NH_2-MIL-125 membrane. It could be observed that a well-intergrown membrane with smooth surface morphology was formed after epitaxial growth (Figure 4c). The cross-sectional SEM image and EDXS pattern indicated that the prepared membrane was only ~90 nm thick (Figure 4d) with no penetration in the substrate pores. EDXS mapping of the Cu element further confirmed that Cu ions were uniformly dispersed in the membrane (Figure 4e). The corresponding XRD pattern (Figure 4f) exhibited only diffraction peaks assignable to (002) and (004) planes, confirming the dominance of *c*-preferred orientation.

It was worth mentioning that besides pore micro-environment engineering, the introduction of Cu ions was indispensable for fine regulating meso-structure of the membrane. Otherwise, substantial twin crystals would be formed on top of the membrane, resulting in a sharp increase in membrane thickness approaching 1.5 μm (Figure S4). Such large discrepancy in meso-structure between membranes prepared in the presence and absence of $Cu(acac)_2$ could be ascribed to different growth kinetics of epitaxial layers. To verify our hypothesis, given amount of Cu@NH_2-MIL-125 NSs were subjected to single-mode microwave heating in the presence of $Cu(acac)_2$ under identical reaction conditions. As shown in Figure S5, the thickness vertical to the (001) plane of Cu@NH_2-MIL-125 NSs was slightly increased to ~110 nm. In contrast, their thickness sharply increased to ~230 nm in the absence of $Cu(acac)_2$, thus confirming the coordination modulation effect of $Cu(acac)_2$ for inhibiting epitaxial growth in the vertical direction.

To fully verify the multi-scale structure superiority, we further fabricated randomly-oriented Cu@NH_2-MIL-125 membrane (denoted as Cu@MIL-M) and *c*-oriented 400 nm-thick NH_2-MIL-125 membrane (denoted as ORI-MIL-M) (Figure S6). The separation performance was evaluated by measuring volumetric flow rates of single gases and binary gas mixtures using the Wicke-Kallenbach technique (Figure S7). Single gas permeation results demonstrated that the ideal C_2H_4/C_2H_6 selectivity reached 13.6, indicating there were few grain boundary defects in the membrane (Table S1). For the C_2H_4/C_2H_6 binary gas mixture, Cu@ORI-MIL-M revealed an unprecedented separation factor (SF) of 12.4 with C_2H_4 permeance of 41 GPU (Figure 5a, Table S2), which represented 925% and 114% enhancement in selectivity and C_2H_4 permeance in comparison with that of ORI-MIL-M (Table S3), demonstrating the validity of π-complexation in efficient C_2H_4/C_2H_6 separation. As shown in Figure 5b, Cu@ORI-MIL-M clearly outperformed state-of-art pure MOF

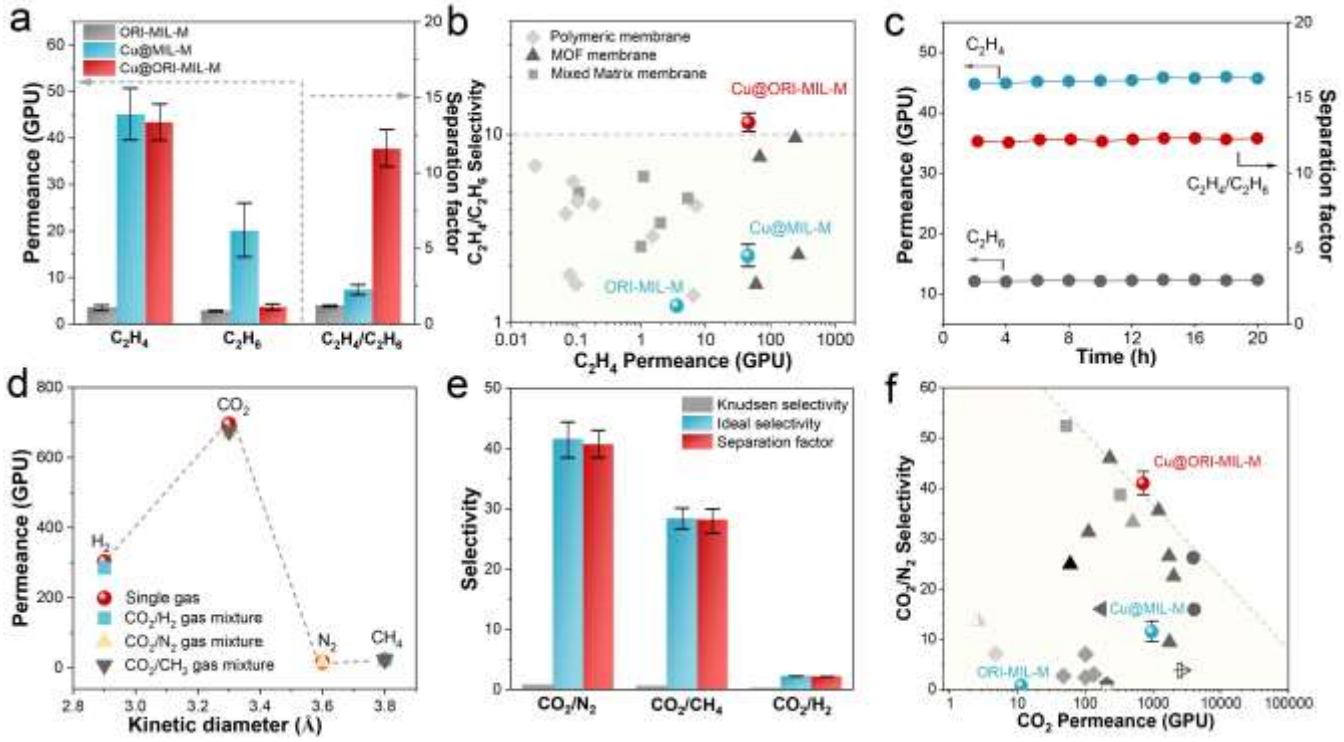

Figure 5. Separation performances of the membranes. a) Separation performance of C_2H_4/C_2H_6 gas pairs through *c*-oriented Cu@NH_2-MIL-125 membrane (Cu@ORI-MIL-M), *c*-oriented NH_2-MIL-125 membrane (ORI-MIL-M) and randomly oriented Cu@NH_2-MIL-125 membrane (Cu@MIL-M). b) Comparison of the C_2H_4/C_2H_6 separation performance of the Cu@ORI-MIL-M with other membranes measured under similar conditions. c) Long-term stability test of Cu@ORI-MIL-M towards equimolar C_2H_4/C_2H_6 gas pair under ambient conditions. d) Single and mixed gas permeances of the Cu@ORI-MIL-M measured under ambient conditions. e) Ideal selectivity and separation factor of different gas pairs through the Cu@ORI-MIL-M. f) Comparison of the CO_2/N_2 separation performance of the Cu@ORI-MIL-M with other pristine pure MOF membranes measured under similar conditions. Detailed data were listed in Table S1-S5. Permeance and selectivity values are averaged over three membranes, and error bars correspond to the standard deviation.

membranes, MOF-based mixed-matrix membranes, and polymer membranes in terms of C_2H_4/C_2H_6 selectivity (Table S4), thus demonstrating outstanding screening accuracy. In addition, orientation control was found crucial for reducing intercrystalline defects, as convinced by inferior separation performance of Cu@MIL-M compared with Cu@ORI-MIL-M (Table S5). Long-term stability of Cu@ORI-MIL-M was further investigated (Figure 5c). After continuous operation for 20 h, both C_2H_4 permeance and C_2H_4/C_2H_6 selectivity remained unchanged, which was indicative of excellent operation stability.

In view of its high affinity for CO_2, the CO_2 separation performance of Cu@ORI-MIL-M was measured further. As shown in Figure 5d, the CO_2 permeance was much higher than other gas molecules. The SF of CO_2/N_2 and CO_2/CH_4 reached 42.3 and 29.6, respectively (Figure 5e, Table S6), which were superior to the majority of pure MOF membranes (Table S7, S8); moreover, its overall CO_2/N_2 separation performance ranked the highest among pristine pure MOF membranes tested under comparable conditions (Figure 5f). To gain insights into the gas transport mechanisms for the CO_2/N_2 and CO_2/CH_4 separations in prepared Cu@ORI-MIL-M, adsorption and diffusion coefficients of different gases in Cu@ORI-MIL-M were further calculated according to the membrane permeability and gas sorption isotherms (Figure S8). It was observed that Cu@ORI-MIL-M showed higher diffusivity coefficient and sorption coefficients for CO_2 than those of N_2 and CH_4 (Table S9). Correspondingly, the Cu@ORI-MIL-M exhibited high diffusivity selectivity (3.88) and solubility selectivity (10.97) for CO_2/N_2; simultaneously, diffusivity selectivity (6.63) and solubility selectivity (4.41) for CO_2/CH_4 was high either. Therefore, excellent CO_2/N_2 and CO_2/CH_4 separation performance could be interpreted by preferential diffusion and adsorption for CO_2 relative to N_2 and CH_4.

Finally, to validate the reproducibility of this approach, two additional Cu@ORI-MIL-M samples were prepared. Gas permeation results indicated that all them exhibited excellent C_2H_4/C_2H_6 and CO_2/N_2 separation performances with small standard deviation (Table S2,S6), that is, CO_2 permeance of 707.6±34.9 GPU with CO_2/N_2 SF of 40.7±2.52 and C_2H_4 permeance of 43.4±4.12 GPU with C_2H_4/C_2H_6 SF of 11.6±1.3, respectively, thereby demonstrating that the synthetic protocol was robust in terms of reproducibility.

Conclusion

To summarize, in this study, we developed a multi-scale structure optimization strategy to prepare highly c-oriented 90 nm-thick Cu@NH_2-MIL-125 membrane. Among various factors, the addition of Cu ions in the precursor solution enabled not only deliberate design of the pore micro-environment, i.e., immobilization of Cu(I) sites in the framework facilitating their π-complexation interactions with C_2H_4 and CO_2, but also fine regulation of the meso-structure (e.g., preferred orientation, thickness, and grain boundary). The multi-scale structure superiority endowed the Cu@NH_2-MIL-125 membrane with C_2H_4/C_2H_6 and CO_2/N_2 separation performance surpassing state-of-the-art pristine pure MOF membranes measured under

comparable conditions, showing great promise for their practical applications.

Acknowledgements

We are grateful to Science Fund for National Natural Science Foundation of China (22108025 and 22078039), the Postdoctoral Science Foundation of China (2021TQ0054), National Key Research and Development Program of China (2019YFE0119200), Science Fund for Creative Research Groups of the National Natural Science Foundation of China (22021005), and the Fundamental Research Fundamental Funds for the Central Universities (DUT22LAB602) for the financial support.

Conflict of Interest

The authors declare no conflict of interest.

Data Availability Statement

Research data are not shared.

Keywords: MOF membrane • nanosheets • gas separation • orientation • π-complexation

[1] a) D. S. Sholl, R. P. Lively, *Nature* **2016,** *532*, 435-437; b) R. P. Lively, D. S. Sholl, *Nature Mater.* **2017,** *16*, 276-279; c) H. B. Park, J. Kamcev, L. M. Robeson, M. Elimelech, B. D. Freeman, *Science* **2017,** *356*, eaab0530; d) S. Yuan, X. Li, J. Zhu, G. Zhang, P. Van Puyvelde, B. Van der Bruggen, *Chem. Soc. Rev.* **2019,** *48*, 2665-2681; e) B. Van der Bruggen, *Nat. Rev. Chem.* **2021,** *5*, 217-218; f) S. Karan, Z. Jiang, A. G. Livingston, *Science* **2015,** *348*, 1347-1351.

[2] a) S. Qiu, M. Xue, G. Zhu, *Chem. Soc. Rev.* **2014,** *43*, 6116-6140; b) Y. Peng, Y. Li, Y. Ban, H. Jin, W. Jiao, X. Liu, W. Yang, *Science* **2014,** *346*, 1356-1359; c) M. S. Denny, J. C. Moreton, L. Benz, S. M. Cohen, *Nat. Rev. Mater.* **2016,** *1*, 16078; d) Q. Qian, P. A. Asinger, M. J. Lee, G. Han, K. Mizrahi Rodriguez, S. Lin, F. M. Benedetti, A. X. Wu, W. S. Chi, Z. P. Smith, *Chem. Rev.* **2020,** *120*, 8161-8266; e) J. Hou, H. Zhang, G. P. Simon, H. Wang, *Adv. Mater.* **2020,** *32*, 1902009; f) A. Knebel, J. Caro, *Nature Nanotech.* **2022,** *17*, 911-923.

[3] L. M. Robeson, *J. Membr. Sci.* **2008,** *320*, 390-400.

[4] a) Y. Liu, Y. Ban, W. Yang, *Adv. Mater.* **2017,** *29*, 1606949; b) Z. Qiao, Y. Liang, Z. Zhang, D. Mei, Z. Wang, M. D. Guiver, C. Zhong, *Adv. Mater.* **2020,** *32*, 2002165; c) C. Wang, Y. Sun, L. Li, R. Krishna, T. Ji, S. Chen, J. Yan, Y. Liu, *Angew. Chem. Int. Ed.* **2022,** 61, e202203663; *Angew. Chem.* **2022**, *134*, e202203663; d) X. Ma, P. Kumar, N. Mittal, A. Khlyustova, P. Daoutidis, K. A. Mkhoyan, M. Tsapatsis, *Science* **2018,** *361*, 1008-1011; e) S. Zhou, O. Shekhah, A. Ramírez, P. Lyu, E. Abou-Hamad, J. Jia, J. Li, P. M. Bhatt, Z. Huang, H. Jiang, T. Jin, G. Maurin, J. Gascon, M. Eddaoudi, *Nature* **2022,** *606*, 706-712.

[5] a) J. B. James, J. Wang, L. Meng, Y. Lin, *Ind. Eng. Chem. Res.* **2017,** *56*, 7567-7575; b) R. Wei, X. Liu, Z. Zhou, C. Chen, Y. Yuan, Z. Li, X. Li, X. Dong, D. Lu, Y. Han, *Sci. Adv.* **2022,** *8*, eabm6741; c) Y. Sun, T. Ji, Y. Gao, J. Yan, Y. He, G. Xu, F. Yan, Q. Bian, Y. Liu, *ACS Materials Lett.* **2023,** *5*, 558-564.

[6] a) J. Yan, T. Ji, Y. Sun, S. Meng, C. Wang, Y. Liu, *J. Membr. Sci.* **2022,** *661*, 120959; b) C. Wang, T. Ji, Y. Wu, G. He, Y. Liu, *ACS Materials Lett.* **2023,** *5*, 1311-1316.

[7] a) N. A. Khan, S. H. Jhung, *J. Hazard. Mater.* **2017,** *325*, 198-213; b) Y. X. Li, W. Zhong, J. J. Zhou, S. C. Qi, X. Q. Liu, L. B. Sun, *Angew. Chem. Int. Ed.* **2022**, *61,* e202212732; *Angew. Chem.* **2022**, *134,* e202212732; c) L. Zhang, L. Li, E. Hu, L. Yang, K. Shao, L. Yao, K. Jiang, Y. Cui, Y. Yang, B. Li, *Adv. Sci.* **2020,** *7*, 1901918.

[8] E. D. Bloch, W. L. Queen, R. Krishna, J. M. Zadrozny, C. M. Brown, J. R. Long, *Science* **2012,** *335*, 1606-1610.

[9] Y. Yin, Z. Zhang, C. Xu, H. Wu, L. Shi, S. Wang, X. Xu, A. Yuan, S. Wang, H. Sun, *ACS Sustain. Chem. Eng.* **2019,** *8*, 823-830.

[10] M. Sun, Q. Gu, A. Hanif, T. Wang, J. Shang, *Chem. Eng. J.* **2019,** *370*, 1450-1458.

[11] a) Y. Yoo, Z. Lai, H.-K. Jeong, *Microporous Mesoporous Mater.* **2009,** *123*, 100-106; b) A. J. Brown, N. A. Brunelli, K. Eum, F. Rashidi, J. Johnson, W. J. Koros, C. W. Jones, S. Nair, *Science* **2014,** *345*, 72-75; c) Y. Sun, Y. Liu, J. Caro, X. Guo, C. Song, Y. Liu, *Angew. Chem. Int. Ed.* **2018,** *57,* 16088-16093; *Angew. Chem.* **2018**, *130*, 16320-16325; d) Q. Hou, S. Zhou, Y. Wei, J. r. Caro, H. Wang, *J. Am. Chem. Soc.* **2020,** *142*, 9582-9586.

[12] a) R. Xu, Y. Kang, W. Zhang, X. Zhang, B. Pan, *Angew. Chem. Int. Ed.* **2022,** *61*, e202115443; *Angew. Chem.* **2022**, *134*, e20215443; b) Y. Sun, J. Yan, Y. Gao, T. Ji, S. Chen, C. Wang, P. Lu, Y. Li, Y. Liu, *Angew. Chem. Int. Ed.* **2023**, *62*, e202216697; *Angew. Chem.* **2023**, *135*, e202216697.

[13] a) M. Dan-Hardi, C. Serre, T. Frot, L. Rozes, G. Maurin, C. Sanchez, G. Férey, *J. Am. Chem. Soc.* **2009**, *131*, 10857–10859; b) S. Yang, L. Peng, S. Bulut, W. L. Queen, *Chem. Eur. J*. **2019**, *25*, 2161–2178.

[14] a) S. Friebe, A. Mundstock, D. Unruh, F. Renz, J. Caro, *J. Membr. Sci.* **2016,** *516*, 185-193; b) Y. Sun, C. Song, X. Guo, S. Hong, J. Choi, Y. Liu, *J. Membr. Sci.* **2020,** *616*, 118615.

[15] Y. Sun, D. Yan, Y. Wu, F.-Y. Shih, C. Zhang, H. Luo, S.-H. Lin, Y. Liu, *ACS Materials Lett.* **2021,** *4*, 55-60.

[16] X. Chen, S. Xiao, H. Wang, W. Wang, Y. Cai, G. Li, M. Qiao, J. Zhu, H. Li, D. Zhang, Y. Lu, *Angew. Chem. Int. Ed.* **2020,** *59*, 17182-17186; *Angew. Chem.* **2020**, *132*, 17335-17339.

[17] Deposition number 751157 (for **MIL-125**) contains the supplementary crystallographic data for this paper. These data are provided free of charge by the joint Cambridge Crystallographic Data Centre and Fachinformationszentrum Karlsruhe Access Structures service.

[18] Y.-X. Li, J.-X. Shen, S.-S. Peng, J.-K. Zhang, J. Wu, X.-Q. Liu, L.-B. Sun, *Nat. Commun.* **2020,** *11*, 3206.

[19] S. Hu, M. Liu, K. Li, Y. Zuo, A. Zhang, C. Song, G. Zhang, X. Guo, *CrystEngComm* **2014,** *16*, 9645-9650.

[20] a) G. Kresse, J. Furthmüller, *Phys. Rev. B* **1996,** *54*, 11169-11186; b) G. Kresse, D. Joubert, *Phys. Rev. B* **1999,** *59*, 1758-1775.

[21] G. Yu, X. Zou, L. Sun, B. Liu, Z. Wang, P. Zhang, G. Zhu, *Adv. Mater.* **2019,** *31*, 1806853.

[22] a) K. V. Agrawal, B. Topuz, T. C. T. Pham, T. H. Nguyen, N. Sauer, N. Rangnekar, H. Zhang, K. Narasimharao, S. N. Basahel, L. F. Francis, C. W. Macosko, S. Al-Thabaiti, M. Tsapatsis, K. B. Yoon, *Adv. Mater.* **2015**, *27*, 3243-3249; b) N. Rangnekar, M. Shete, K. V. Agrawal, B. Topuz, P. Kumar, Q. Guo, I. Ismail, A. Alyoubi, S. Basahel, K. Narasimharao, C. W. Macosko, K. A. Mkhoyan, S. Al-Thabaiti, B. Stottrup, M. Tsapatsis, *Angew. Chem. Int. Ed.* **2015**, *54*, 6571-6575; *Angew. Chem.* **2015**, *127*, 6671-6675; c) M. Y. Jeon, D. Kim, P. Kumar, P. S. Lee, N. Rangnekar, P. Bai, M. Shete, B. Elyassi, H. S. Lee, K. Narasimharao, S. N. Basahel, S. Al-Thabaiti, W. Xu, H. J. Cho, E. O. Fetisov, R. Thyagarajan, R. F. DeJaco, W. Fan, K. A. Mkhoyan, J. I. Siepmann, M. Tsapatsis, *Nature* **2017**, *543*, 690-694; d) D. Kim, M. Y. Jeon, B. L. Stottrup, M. Tsapatsis, *Angew. Chem. Int. Ed.* **2018**, *57*, 480-485; *Angew. Chem.* **2018**, *130*, 489-494; e) D. Kim, S. Ghosh, N. Akter, A. Kraetz, X. Duan, G. Gwak, N. Rangnekar, J. R. Johnson, K. Narasimharao, M. A. Malik, S. Al-Thabaiti, B. McCool, J. A. Boscoboinik, K. A. Mkhoyan, M. Tsapatsis, *Sci. Adv.* **2022**, *8*, eabm8162.

[23] Y. Sun, L. Liu, T. Ji, J. Yan, Y. Liu, *Chem. Commun.* **2022,** *58*, 8822-8825.

10.1002/anie.202311336

WILEY-VCH

Entry for the Table of Contents

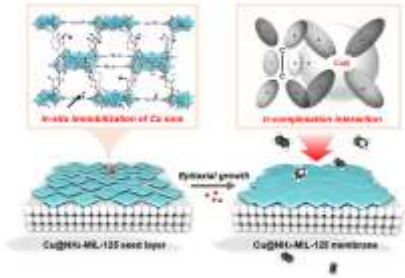

A multi-scale structure optimization strategy gives an oriented ultrathin NH_2-MIL-125 metal-organic framework (MOF) membrane chelated with coordinatively unsaturated Cu ions. Cu ions act as coordinating modulator and recognition sites, enabling the formation of ultrathin nanosheets and membranes. They also promote π-complexation interactions with C_2H_4 and CO_2, leading to enhanced performance for ethylene/ethane and flue gas separations.